

# **PAPER • OPEN ACCESS**

# Thermally induced changes in the elastic properties of prostatic tissue: a preliminary study on *ex vivo* bovine samples

To cite this article: Leon Zurfluh et al 2025 Phys. Med. Biol. 70 215001

View the article online for updates and enhancements.

# You may also like

- Averaged Disturbing Function for the Saturn-Titan-Hyperion 4:3 Resonance Letícia Guimarães Silva
- Committed acceleration of climate stresses in the coming decades Noah S Diffenbaugh
- <u>Study of Optical Properties of MOCVD-Grown Rutile GeO 2 Films</u> Inteaz Rahaman, Anthony Bolda, Botong Li et al



# Physics in Medicine & Biology





# PAPER

#### **OPEN ACCESS**

#### RECEIVED

1 May 2025

#### REVISED

1 October 2025

#### ACCEPTED FOR PUBLICATION

9 October 2025

#### PUBLISHED

21 October 2025

Original Content from this work may be used under the terms of the Creative Commons Attribution 4.0 licence.

Any further distribution of this work must maintain attribution to the author(s) and the title of the work, journal citation and DOI.



# Thermally induced changes in the elastic properties of prostatic tissue: a preliminary study on *ex vivo* bovine samples

Leon Zurfluh<sup>1,2</sup>, Antonio Callejas<sup>1,2,3</sup> and Antonio Gomez<sup>1,2,3,4,\*</sup>

- Department of Structural Mechanics and Hydraulic Engineering, University of Granada, Granada 18071, Campus de Fuentenueva S/N, Spain
- TEC-12 Group, Biosanitary Research Institute, ibs.Granada, Granada 18012, Avenida de Madrid 15, Spain
- <sup>3</sup> Excellence Research Unit 'ModelingNature' (MNat), University of Granada, Granada 18071, Campus Fuentenueva S/N, Spain
- $^4\,$  UCL Mechanical Engineering, University College London, London WC1E 7JE, United Kingdom
- \* Author to whom any correspondence should be addressed.

E-mail: ajgomez@ugr.es

Keywords: thermal ablation, elasticity change, shear wave elastography, prostate

Supplementary material for this article is available online

# **Abstract**

Objective. To characterise the thermally induced changes in the elastic properties of prostatic tissue and investigate their correlation with thermal dose. *Approach. Ex vivo* bovine prostate samples were subjected to three heating protocols—constant-rate heating, steady-state temperature, and steady-state temperature followed by rapid cooling. Acoustic Radiation Force-based Shear Wave Elastography was used to monitor shear wave speed (SWS), and the results were interpreted in relation to thermal dose using the cumulative equivalent minutes at 43 °C (CEM43) scale. *Main results*. Thermal exposure consistently resulted in increased SWS, with increments of up to five-fold observed at temperatures above 60 °C in the constant-rate heating tests. Irreversible changes were also observed in the steady-state temperature test followed by rapid cooling even at thermal exposures as low as 20 CEM43 min. *Significance*. These findings support the potential of elastography to delineate thermally ablated regions in prostate cancer treatment and encourages further investigation on the potential of SWS to serve as a biomarker of thermal dose.

# 1. Introduction

Prostate cancer is a significant health concern due to its high incidence and mortality rates. It is the most common cancer in men across 112 countries, accounting for 15% of all diagnosed cancers (James et al 2024). Increasing attention has been directed toward focal therapies, which aim to selectively target pathological tissue while preserving surrounding healthy tissue (Arcot and Polascik 2022, Basseri et al 2024). Among these, focal thermal ablation, a form of hyperthermia, achieves coagulative necrosis of tissue by inducing elevated temperatures—typically in the range of 50 °C–80 °C within the target tissue (Geoghegan et al 2022, Basseri et al 2024). Current focal thermal ablation modalities include high-intensity focused ultrasound (HIFU), radiofrequency ablation, microwave ablation, and laser interstitial thermal therapy, all of which generate confined zones of tissue destruction, resulting in fewer complications than conventional cancer therapies (Geoghegan et al 2022). Despite their demonstrated efficacy, focal thermal therapies for prostate cancer still face a critical technical challenge: accurately assessing the delivered thermal dose and the extent of the lesion (van der Poel et al 2018, Geoghegan et al 2022).

After thermal ablation, the treated tissue exhibits increased stiffness compared to the non-ablated tissue (Kiss *et al* 2009, Sapin-de Brosses *et al* 2010, 2011, Mariani *et al* 2014, Shi *et al* 2015, Payen *et al* 2024). This stiffness contrast motivates the use of elastography imaging to assess the lesion. Elastography encompasses a range of medical imaging techniques that map the elasticity of soft tissues by analysing their mechanical response to external forces (Bamber *et al* 2013, Sigrist *et al* 2017). Among the various elastography modalities, acoustic radiation force-based shear wave elastography (ARF-SWE) is the most widely used. ARF-SWE, hereinafter referred to as SWE, utilises ultrasound-induced ARF to

remotely generate shear waves, which are tracked to derive the elastic properties of tissue, typically by measuring the group shear wave speed (SWS) (Nightingale et al 2003, Bercoff et al 2004).

Several studies have explored the use of elastography to image thermal ablation in prostate cancer. One of the most recent studies is the work by Payen et al (2024), which investigated passive elastography for imaging HIFU-ablated tissue. The study tested this approach on ex vivo bovine liver, in vivo porcine liver, and in vivo human prostates. In the ex vivo bovine liver experiments, the HIFU lesions were significantly stiffer than untreated tissue, with a shear wavelength contrast ratio of 2.5, corresponding to a 6-fold increase in stiffness. The *in vivo* porcine liver tests showed shear wavelength increases of up to four times. In the in vivo human prostate cases, results were variable: in two patients, tumours initially stiffer than surrounding tissue appeared softer after ablation, while in the other two, tumours exhibited a 1.5-fold increase in shear wavelength after ablation. These findings, while relevant, should be interpreted cautiously due to the small sample size. Other work considering the alteration in mechanical properties of prostate after HIFU ablation was carried out by Gomez et al (2023). They developed a computational approach to reconstruct the location and quantify alterations in the viscoelastic properties of HIFU-induced lesions in the prostate. They assumed a 6-fold increase in SWS based on findings from studies on other glandular tissues, given the absence of data for prostatic tissue in the literature. Other elastography studies assessing HIFU ablation of prostate cancer have been limited to strain elastography (Souchon et al 2003, Curiel et al 2005), an elastography modality that does not provide quantitative results for the change in stiffness.

Thermal ablation, and hyperthermia more broadly, depend on the heating history -i.e. the combination of temperature and exposure time- quantified through a metric known as thermal dose. Several methods have been proposed to quantify thermal dose, with the cumulative equivalent minutes at 43 (CEM43) scale introduced by Sapareto and Dewey (1984) being the most widely used. For biological tissues, the thermal dose required to achieve coagulative necrosis typically ranges from 25 to 240 min at 43 °C (Dewhirst *et al* 2003). However, the applicability of the CEM43 scale diminishes as the temperature deviates further above the 43 °C (Assi *et al* 2022).

If thermal ablation alters the elastic properties of ablated prostatic tissue, it is reasonable to assume that both temperature and time contribute to these changes. This underscores the need for a thorough characterisation of how the elasticity of prostatic tissue evolves with thermal dose. To date, no studies have explored this fundamental relationship in prostatic tissue; however, similar analyses have been conducted in other types of soft tissue. Kiss et al (2009) observed complex trends in the Young's modulus of ex vivo canine and porcine livers treated with radiofrequency ablation, identifying local maxima at 70 °C-75 °C, followed by decreases at higher temperatures, attributed to collagen denaturation. Sapin-de Brosses et al (2010) reported a distinct three-stage pattern in the shear modulus of ex vivo bovine muscle in a thermal water bath, though inconsistent trends were observed in liver tissue. Their follow-up study in in vivo rat leg muscle (Sapin-de Brosses et al 2011) demonstrated correlation between thermal dose and stiffness, with an eight-fold increase at 202 min CEM43. In other in vivo test, Mariani et al (2014) assessed radiofrequency thermal ablation of porcine livers using SWE, establishing a Young's modulus threshold of 20 kPa to predict ablative necrosis with high accuracy. Shi et al (2015) highlighted differences between in vivo and ex vivo liver radiofrequency ablation experiments, noting tissue softening in the ex vivo experiments but not in vivo, likely due to the cooling effect of perfusion. Although not relevant for hyperthermia, Arnal et al (2011a, 2011b) showed a temperature-shear modulus softening relationship of  $-1.0 \,\mathrm{kPa}\,^{\circ}\mathrm{C}^{-1}$  between 30 °C-40 °C in ex vivo turkey muscle using SWE. These findings support the hypothesis that a relationship may exist between thermal dose and elasticity, specific to each tissue

Understanding the correlation between elasticity and thermal dose is essential for optimising elastography modalities in the monitoring and assessment of thermal ablation as a prostate cancer treatment. This preliminary study aims to characterise the changes in the mechanical properties of prostatic tissue induced by thermal exposure using an *ex vivo* animal tissue model. While contributing to the fundamental understanding of thermal effects on prostatic tissue mechanics, this initial stage primarily focuses on identifying key trends rather than establishing definitive quantitative conclusions.

The remainder of this paper is organised as follows. The methodology section describes the experimental procedures designed to investigate temperature-dependent changes in the mechanical properties of *ex vivo* bovine prostatic tissue. Subsequently, results from three distinct heating protocols are presented, each providing insights into specific aspects of the impact of thermal ablation on elastic properties. Finally, the discussion explores the implications of these findings and outlines potential directions for future research.

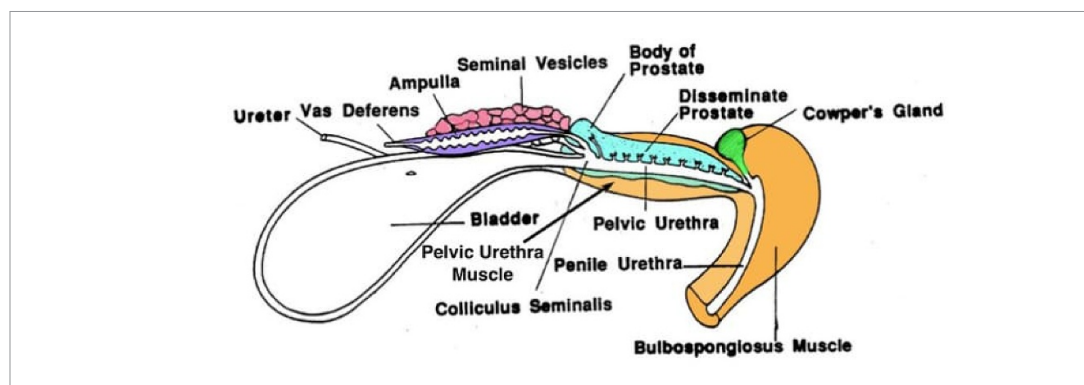


**Figure 1.** Anatomical diagram of the uro-reproductive system of a bull, illustrating the location of the prostate regions. Reproduced with permission from University of Wisconsin-Madison, Department of Animal Sciences (n.d.), figure is titled "Pelvic Genitalia of the Bull".

# 2. Methodology

# 2.1. Ex vivo bovine prostate samples

Canine subjects are frequently used as animal models in prostate cancer research (LeRoy and Northrup 2009, Mitri *et al* 2011); however, due to personal ethical concerns, *ex vivo* bovine prostatic samples were used instead. These samples were sourced from animals fit for human consumption at local abattoirs. The breed of the animals was not recorded, except for four samples identified as 'toro de lidia', an Iberian bull breed traditionally raised for bullfighting, whose carcasses are also processed for human consumption following the bullfight. Ethical approval was granted from the university's ethics committee. The animals included in the study differed in age, with those specifically raised for meat production being approximately 12 months old, while the 'toro de lidia' specimens were older (age shown in the results figure 4). The age and the breed of the animals were not differentiating factors, which is demonstrated in the results section. None of the animals had been sterilised. Samples were collected following veterinary inspection, shortly after slaughter, and were transported refrigerated to our laboratory facilities. The tests were conducted within 2–4 h post-mortem.

As in humans, the bovine prostate surrounds the urethra at the neck of the urinary bladder; however, its geometry differs significantly (see figure 1). The bovine prostate comprises two distinct parts: a firm protuberance known as the body of the prostate (BP) and a maximum 5 mm thick, elongated, soft annular layer called the disseminated prostate (DP). The DP also includes the culliculus seminalis (verumontanum), where the vas deferens and seminal vesicles converge into the urethra, similarly to the human prostate. Upon manual palpation, the BP exhibited a hard consistency comparable to that of nasal cartilage. Consequently, the characterisation tests focused on the DP, including the region of the culliculus seminalis. Surrounding the DP is the annular structure of the pelvic urethra muscle (PUM) (see figure 1). In our initial tests, this muscular structure exhibited elasticity values similar to those of the DP region, likely because the muscle fibres were not aligned with the shear waves generated. Prior to testing, the samples were sectioned longitudinally along the urethra to expose the inner surface of the urethral conduit, resulting in a bilayer structure with the DP region lying on top of the PUM layer (see figure 2).

#### 2.2. Experimental setup

The experimental setup consisted in a temperature-monitored water bath that allowed exposition of the samples to thermal dose with simultaneous performance of SWE (see figure 3(a)). The setup was designed to allow the water bath to reach temperatures ranging from room temperature  $(25\,^{\circ}\text{C})$  up to  $70\,^{\circ}\text{C}$ .

Following a similar approach to that used by Sapin-de Brosses *et al* (2010), the temperature-monitored water bath consisted of a 1 L borosilicate beaker placed on a hot plate. Two temperature sensors were immersed in the bath at the same depth and in close proximity to the sample, to provide continuous temperature monitoring (see figure 3(a)). Although the hot plate was manually controlled, the system's heating response was characterised and adjusted to achieve the desired temperature protocol for each test. The temperature sensors used in the tests were DS18B20 (Texas Instruments), which have a specified accuracy of  $\pm 0.5$  °C according to the manufacturer's datasheet. Each temperature reading was computed as the average of the two probes, with each probe output representing the mean of

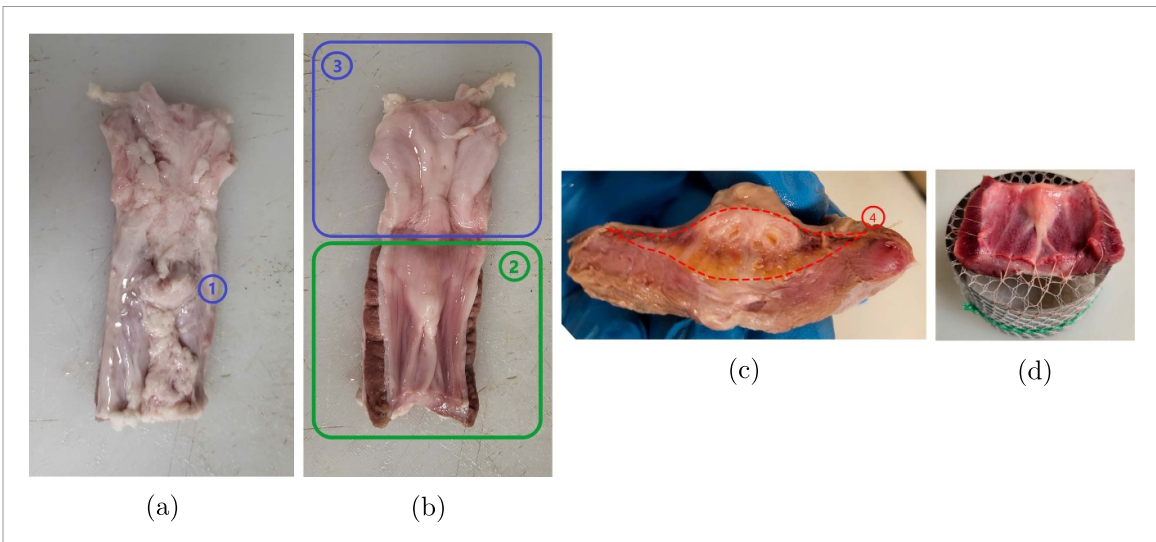


**Figure 2.** Sample sectioned longitudinally along the urethra on the side opposite to the BP. (a) Outer side of the urethral structure, with (1) indicating the BP location beneath the adipose tissue; (b) inner side of the urethral structure, with (2) highlighting the DP region overlying the PUM, and (3) showing a portion of the bladder wall; and (c) cross-sectional view of the DP-PUM bilayer, with (4) illustrating the DP structure. (d) Sample stitched to the net in the supporting frame.

three consecutive measurements acquired at one-second intervals. This measurement approach was calibrated against two reference thermometers, yielding a maximum deviation of  $\pm 0.2$  °C.

Each sample was trimmed to ensure consistent geometry across all tested samples. The perimeter was then stitched onto a cotton net using thread (see figure 2(d), which was subsequently attached to a circular metal frame, positioning the sample 5 cm above the bottom of the beaker (figure 3(a)).

SWE by a Vantage 256 system (Verasonics, Kirkland, WA, USA) and an L11-5 V ultrasound transducer (Verasonics, Kirkland, WA, USA) was used to characterise the SWS of the samples. To maintain the transducer below 45 °C as instructed by the probe manufacturer, a custom-made secondary water container with a water recirculation system and an acoustic window at its bottom was employed (see figure 3(a)). The maximum temperature measured in the secondary container during the tests was 41 °C. The container was mounted on a computer-controlled mechanism that enabled rapid vertical motion. The container was submerged in the temperature-monitored water where the sample was exposed to the thermal dose to perform the SWE measurement. Temperature and time of each measurement were recorded. The container's stopping position was calibrated so that the ARF focus targeted the DP of the sample.

# 2.3. Quantification of the thermal exposure

During the thermal exposure tests, temperature measurements were recorded at 1-minute intervals, matching the frequency of the SWE acquisitions. The entire SWE acquisition protocol was optimised to reach this sampling rate, which was accomplished by parallelising the motion of the transducer container and the data saving processes. The collected data were analysed to estimate the SWS of the samples as a function of time and temperature, based on the thermal isoeffect dose CEM43, see equation (1) (Sapareto and Dewey 1984). The CEM43 scale represents the equivalent time, in minutes, that biological tissue would need to be exposed to a temperature of 43 °C to induce thermal damage.

$$CEM43 = \sum_{i=1}^{n} t_i R^{(43-T_i)}$$
 (1)

where  $t_i$  represents the time points and  $T_i$  the temperature at each corresponding time point. The parameter R denotes the number of minutes required to compensate for a 1 °C temperature change to achieve the equivalent thermal damage effect at 43 °C. Sapareto and Dewey (1984) assigned R a fixed value of 0.5 when  $T_i$  is above 43 °C and 0.25 when it is below. However, as noted by previous studies (Bhowmick *et al* 2004, van Rhoon 2016, Assi *et al* 2022) and demonstrated in this study (see the supplementary corresponding figures), using R = 0.5 results in excessively high CEM43 values at temperatures exceeding 47 °C–50 °C. Notably, Sapareto and Dewey (1984) acknowledged that R could vary between 0.4 and 0.8 for temperatures above 43 °C. In reality, R is both temperature- and tissue-dependent (see equation (2)), as indicated by Henriques and Moritz (1947), who first applied the Arrhenius model to

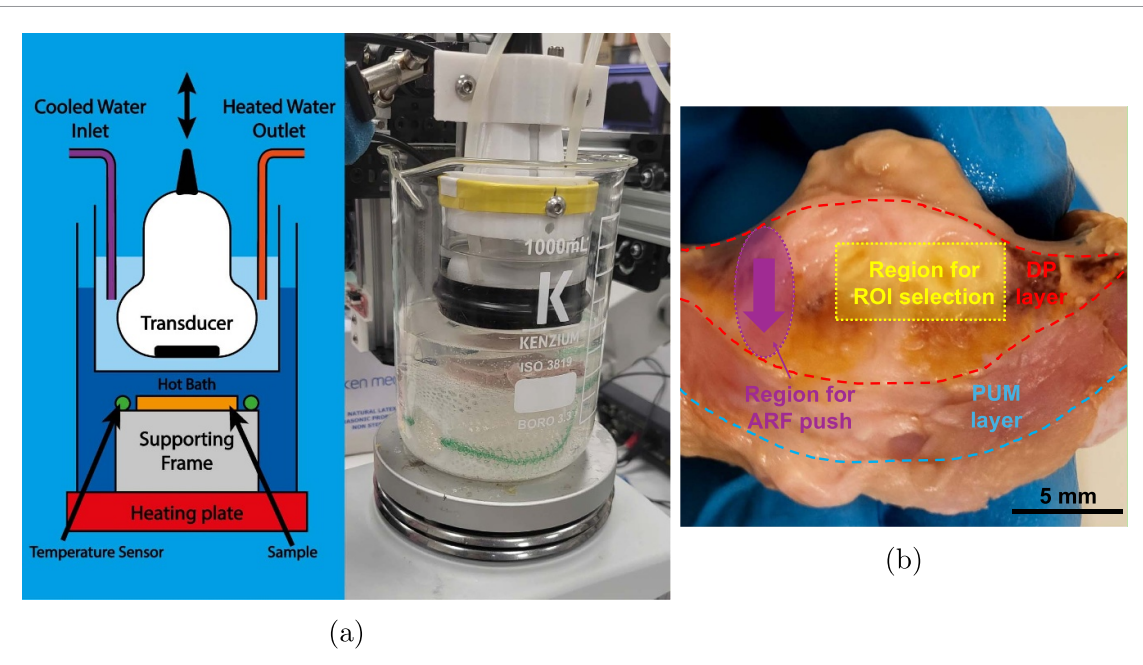


Figure 3. (a) Schematic of the experimental setup. (b) Cross-section of a sample illustrating the approximate region used for generating the ARF push and for the Region of Interest (ROI) selection ( $\approx 4 \times 8$  mm), where the SWS analysis is performed; see section 2.4.

hyperthermia-the basis from which the CEM43 scale is derived.

$$R = e^{-E_a/\left(R_g T_K(T_K + 1)\right)} \tag{2}$$

where  $E_a$  is the activation energy barrier (cal/mol),  $R_g$  is the universal gas constant (1.987 cal mol<sup>-1</sup> °K), and  $T_K$  is the absolute temperature (°K) (Sapareto and Dewey 1984, Dewhirst *et al* 2003, Bhowmick *et al* 2004).

In this work, the value of R was taken as indicated by Sapareto and Dewey (1984) for temperatures below 43 °C. For temperatures above 43 °C, R was calculated according to equation (2) using the activation energy parameter  $E_a = 42.6 \,\mathrm{kcal} \,\mathrm{mol}^{-1}$ , as experimentally fitted for  $ex \, vivo$  human prostatic tissue from radical prostatectomy in the study by Bhowmick  $et \, al \, (2004)$ . For the range of temperatures tested (up to 70 °C), equation (2) yielded values of R from 0.8 to 0.83 (applied to temperatures above 43 °C).

# 2.4. SWE and estimation of the SWS

The elastic properties of the samples were characterised using the group velocity of the propagated shear waves, referred to as the SWS. The SWS can be considered a measure of the stiffness of the medium as it is proportional to the square root of the shear modulus. Beamformed IQ data from the Verasonics Vantage 256 system was used to estimate particle displacement across a sequence of temporal frames using the Loupas correlation algorithm (Loupas *et al* 1995). Five ROIs were manually selected by the same operator within a defined area of analysis of approximately  $4\times8$  mm within the DP region of the samples, carefully avoiding the chaotic focal region of the ARF (a schematic is shown in figure 3(b)). Each ROI extended up to 8 mm along the direction of shear wave propagation. Transversely, the ROIs measured up to 1 mm. In image pixel terms, the ROI size ranged from  $10\times80$  to  $20\times100$  pixels, with the first dimension aligned with the ultrasound beam (i.e. vertical dimension in figure 3(b). The pixel size was  $4.8\times9.8~\mu$  m. The SWS value was computed as the slope of the leading edge formed by the maximum particle displacement at each position across the sequence of frames. The data points and the whiskers in the results figures correspond to the mean and standard deviation calculated across the five analysed ROIs.

SWS characterisation was terminated when the reconstructed values became unreliable due to an excessive number of outliers deviating from the tendency curve. This situation occurred either as a result of a poor signal-to-noise ratio (SNR<3) or because the sample shifted out of the ARF focus due to extreme permanent thermal shrinkage.

Given the dimensions of the samples and their layered structure, it is likely that guided modes of propagation were excited, with the Scholte wave predominating on the surface of the samples (Scholte

1947). However, these waves were not explicitly accounted for in the analysis. If present, their velocity-approximately 84% of the SWS (Li *et al* 2019)-fell within the experimental variability of the SWS measurements. Moreover, since the analysis focused on relative changes in SWS due to thermal exposure, the potential influence of guided waves on absolute SWS values was minimised.

#### 2.5. Temperature protocols

Thermal dose does not depend linearly on time or temperature (equation (1)) (Sapareto and Dewey 1984). Following a similar approach to that of Sapin-de Brosses *et al* (2010, 2011), three types of tests were conducted under different temperature histories.

# Test type 1: constant-rate heating

The first type of test employed a temperature protocol with a constant, linearly increasing ramp at a rate of 1 °C min<sup>-1</sup>, starting from room temperature and reaching up to 70 °C. Eight samples were analysed. Four of them were obtained from 'toro de lidia' specimens, while the rest were obtained from animals of approximately 12 months of age raised for meat production. These tests pursued the identification of the temperature at which noticeable changes in SWS occurred.

# Test type 2: steady temperature

The second type of test investigated the temperature-dependent behaviour of SWS under uniform temperature conditions. It focused on the range of temperatures for which the CEM43 scale was originally conceived (Sapareto and Dewey 1984), within which changes in SWS began to be observed in test type 1. Samples were submerged in a pre-heated, temperature-stable water bath. Seven samples were analysed, with tests conducted at temperatures ranging from 43 °C to 53 °C. All samples tested under this protocol were obtained from animals raised for meat production and approximately 12 months of age.

#### Test type 3: steady temperature followed by rapid cooling down

Thermal ablation induces irreversible changes in the elastic properties of tissue. However, irreversibility of these changes is not clear at lower thermal doses (Sapin-de Brosses *et al* 2010). The third type of test evaluated the residual change in elastic property if thermal exposure is suddenly dropped off. The temperature protocol consisted of maintaining a steady temperature plateau at around 43 °C, followed by a rapid cooling phase achieved by submerging the samples in a secondary container filled with water maintained at 25 °C. Four tests were conducted, initiating the cooling phase at four different times: 20, 40, 60 and 120 min. In all cases, the cooling phase spanned 30 min. The time needed to restart the ARF-SWE tests after immersing the sample in the cold bath was approximately 2 min. All samples tested under this protocol were obtained from animals raised for meat production and approximately 12 months of age.

# 3. Results

# 3.1. Constant-rate heating

Results from this test are shown in figure 4(a). For each sample, five SWS analyses were performed, with the mean values and standard deviation (whiskers) represented in the graph. Considerable variability in SWS behaviour among samples was observed as temperature increased, with this variability growing with temperature, reaching up to 50% relative to the mean SWS value across the eight samples at a given temperature point. A moderate correlation (Pearson r = 0.5925) was found between the animal's age and SWS at initial temperatures (i.e. before thermal injury, below 40 °C), but this correlation diminished to near zero at 65 °C (Pearson r = 0.0251).

Initial SWS values ranged from 1.5 to 2.8 m s<sup>-1</sup>. Overall, an increase in SWS was observed in all cases, with increments reaching up to five times the initial SWS value. However, the rate of increase exhibited a distinct pattern across the temperature range. Between room temperature and 40 °C, no appreciable changes in SWS were noticeable beyond the observed measurement variability. From 40 °C to 50 °C, SWS began to increase gradually, but not more than 50% of the initial SWS value. Between 50 °C and 60 °C, the rate of change accelerated, and above 60 °C, SWS increased sharply, reaching increments of up to five times the initial value. It is important to note that these results are specific to a heating rate of 1 °C per minute. Different heating profiles, as demonstrated in test type 2, may yield different outcomes.

In figure 4(b), the results from figure 4(a) were normalised to the measurements at the initial time points at room temperature. Furthermore, time and temperature were combined into a single metric using the modified CEM43 scale based on the parameters from Bhowmick *et al* (2004) (equations (1)

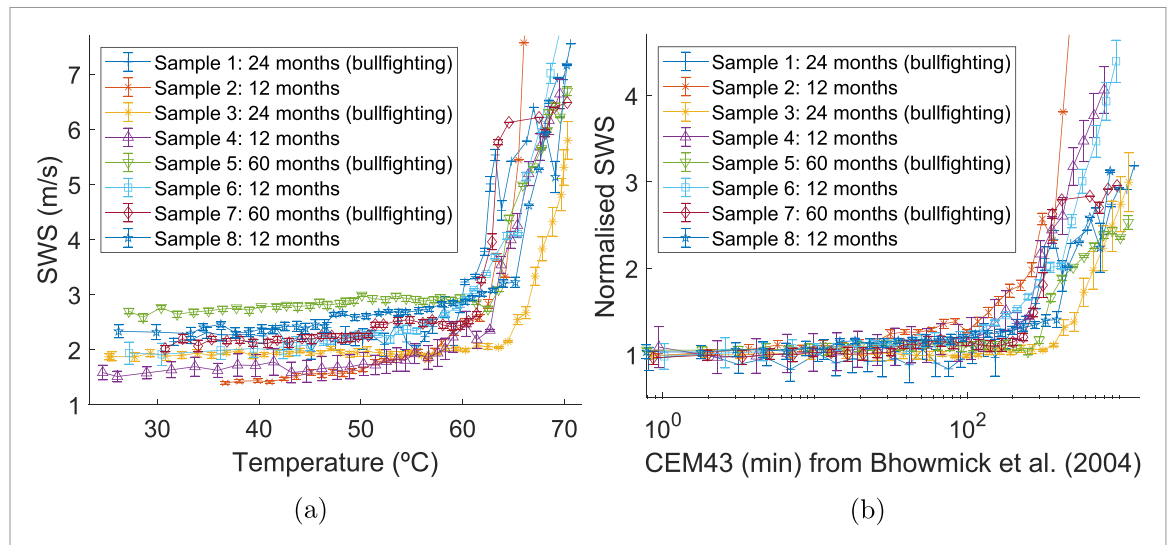


**Figure 4.** SWS measurements from *ex vivo* bovine prostatic samples during constant-rate heating test at 1 °C/min, shown as (a) function of temperature and (b) function of thermal exposure using the modified CEM43 scale using the parameters from Bhowmick *et al* (2004) (horizontal axis in logarithmic scale). Data points and whiskers correspond with the mean and standard deviation of SWS estimation over 5 different ROIs.

and (2)). An initial attempt to use R = 0.5, as originally proposed by Sapareto and Dewey (1984) and employed in various reference studies, such as that by Sapin-de Brosses *et al* (2011), resulted in incoherently high CEM43 values, reaching the order of  $10^8$  CEM43 min (the respective figure is within the supplementary material). This demonstrates that the CEM43 scale as employed by Sapareto and Dewey (1984) fails to represent thermal exposure at temperatures exceeding 45 °C), as discussed in other studies (Bhowmick *et al* 2004, van Rhoon 2016, Assi *et al* 2022). Alternatively, using R calculated as described in the methodology section 2.3 and based on the parameters determined by Bhowmick *et al* (2004) for prostatic tissue, for temperatures above 43 °C, yielded CEM43 min that were more consistent with the expected times for thermal injury: not more than a few hundred CEM43 min (van Rhoon 2016, Geoghegan *et al* 2022). The dispersion of stiffening trends, defined as SWS increases relative to initial values, increased with thermal dose (see figure 4(b)).

# 3.2. Steady temperature

Results from this test are shown in figure 5. Figure 5(a) presents the absolute SWS values as a function of heat exposure time, including the initial SWS values at room temperature, which ranged from 1.5 to  $2.5\,\mathrm{m\,s^{-1}}$ . In all cases, SWS began increasing almost immediately, within the first 2 min of immersion in the water bath. After the initial 10–20 min, SWS exhibited an approximately linear increase over time. Final SWS increments ranged from 50% to 130%, aligning with the order of magnitude observed in test type 1 for temperatures between 40 °C and 55 °C (see figure 4(a)). The duration of each test was limited by the quality of the reconstructed SWS values. After 90–100 min, the water in the hot bath began to cloud due to the diffusion of impurities from the samples, reducing the SNR of the ultrasound signals and degrading the quality of wave propagation measurements, ultimately forcing the termination of the tests. The gradual and continuous change in SWS observed here contrasts with the sudden increase noted in test type 1 at temperatures above 60 °C.

Figure 5(b) presents the SWS values from figure 5(a) normalised by the SWS value at room temperature. The linear rate of SWS change over time did not show a significant correlation with temperature (Pearson r = 0.4093). The stiffening trends over time with samples exposed to constant temperatures between 43 °C–53 °C displayed similar slopes, irrespective of the temperature. However, this should be interpreted cautiously given the narrow temperature range tested and the limited sample size.

Figure 5(c) shows the SWS values normalised to their respective measurements at room temperature and expressed as a function of thermal dose, calculated using the modified CEM43 scale by the parameter R as defined in equation (2) (Bhowmick *et al* 2004). As observed in figure 5(b), a consistent increase in SWS was evident across all samples and temperatures as thermal exposure progressed. Variability among samples increased over time, further highlighting the complexity of the tissue response to thermal exposure. Notably, two distinct trend groups emerged: one for tests conducted below  $50\,^{\circ}$ C and another for those above this threshold. The separation became more pronounced when using the

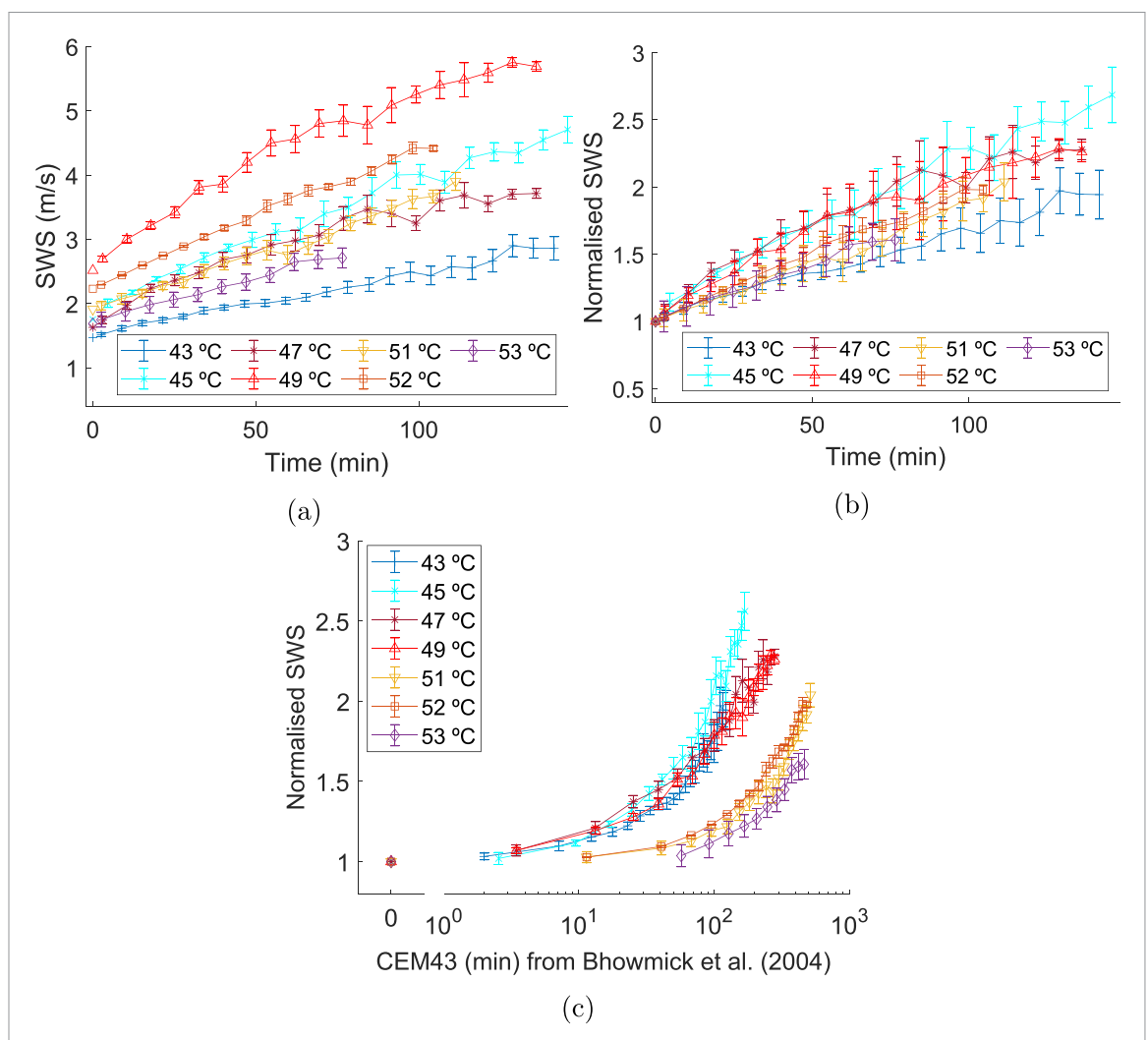


**Figure 5.** SWS measurements from *ex vivo* bovine prostatic samples during the steady temperature test (test type 2), shown as (a) function of exposure time to heat, (b) normalised by the SWS value at room temperature and as a function of exposure time to heat, and (c) normalised by the SWS value at room temperature and as a function of thermal exposure using the modified CEM43 scale using the parameters from Bhowmick *et al* (2004) (horizontal axis in logarithmic scale). Data points and whiskers correspond with the mean and standard deviation of SWS estimation over 5 different ROIs.

original R values proposed by Sapareto and Dewey (1984), as shown in the supplementary material. This separation appears to stem primarily from the mathematical definition of the CEM43 scale (equation (1)), and therefore no clear relationship between CEM43 and SWS can be established for the range of temperatures tested (43 °C–53 °C).

# 3.3. Steady temperature followed by rapid cooling down

Results from this test are shown in figure 6, with SWS values normalised to their initial measurements at room temperature. Consistent with test type 2, SWS began increasing within the first two min after immersion in the water bath at  $43\,^{\circ}$ C. Similarly, after the initial 10– $20\,\mathrm{min}$ , the rate of change in SWS stabilised, showing a nearly constant increase over time. In all cases, this steady rise was followed by a stable plateau once the cooling phase began, persisting throughout the entire 30-minute cooling period and indicating an irreversible change. The transition time from the hot to the cold bath was accounted for in the graphs. The results show a clear correlation between the magnitude of irreversible change and the duration of thermal exposure (Pearson r = 0.9868), with longer heating times leading to greater increases in SWS, from a 20% increase for the 20 min test to 50% for the 120 min test. In two cases, corresponding to 40 and 120 min of thermal exposure, the cooling phase appeared to show a slight softening, represented by a small decrease in SWS. However, this decrease falls within the observed standard deviation after cooling, likely reflecting the natural variability of SWS measurements and minor differences in ROIs placement between the thermal exposure and cooling phases.

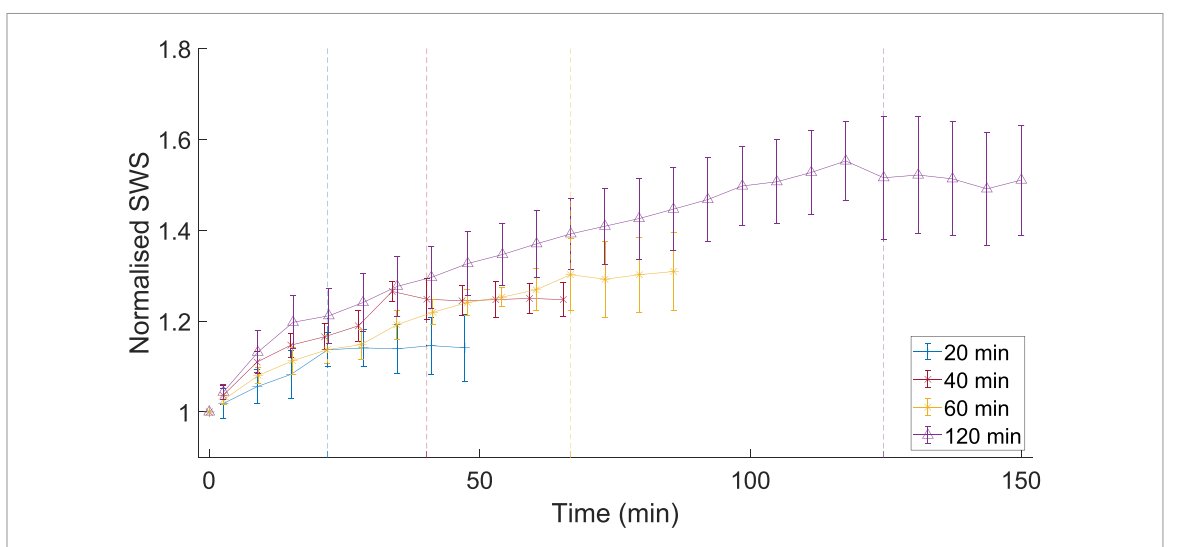


**Figure 6.** Normalised SWS measurements by their respective SWS value at room temperature, as a function of time, from *ex vivo* bovine prostatic samples during the steady temperature test at 43 °C followed by rapid cooling down. Thermal exposure times were 20, 40, 60 and 120 min followed by 30 min of cooling phase. The dash vertical line separates the thermal exposure phase from the cooling down phase. Data points and whiskers correspond with the mean and standard deviation of SWS estimation over five different ROIs.

# 4. Discussion

This study investigated the impact of thermal exposure on the elastic properties of prostatic tissue, using for that purpose  $ex\ vivo$  bovine prostates. Three type of tests explored different thermal exposure profiles to assess changes in SWS, following similar procedures from the literature (Sapin-de Brosses  $et\ al\ 2010$ , 2011, Amador  $et\ al\ 2015$ ). Test type 1 used a constant heating rate of  $1\,^{\circ}\text{C}\ \text{min}^{-1}$  up to  $70\,^{\circ}\text{C}$  to identify temperature thresholds for SWS changes. Test type 2 maintained steady temperatures between  $43\,^{\circ}\text{C}$  and  $53\,^{\circ}\text{C}$  to capture temperature-dependent behaviour at the interval where changes in SWS become significant. Test type 3 held a steady temperature at  $43\,^{\circ}\text{C}$  followed by rapid cooling to  $25\,^{\circ}\text{C}$ , evaluating the irreversibility of stiffness changes after varying thermal doses. In addition, the CEM43 scale proposed by Sapareto and Dewey (1984) was used in this study to quantify thermal dose by combining time and temperature into an equivalent exposure at  $43\,^{\circ}\text{C}$ . To address the scale's known limitations at high temperatures, the parameter R was adjusted based on the Arrhenius model, using experimentally fitted activation energy for prostatic tissue from Bhowmick  $et\ al\ (2004)$ , which yielded more coherent CEM43 values for temperatures above  $43\,^{\circ}\text{C}$ .

The temperature ranges tested (up to  $70\,^{\circ}$ C) induced notable changes in SWS, with the largest increments observed at higher temperatures (see figure 4(a)). Above  $60\,^{\circ}$ C, SWS increased between two and five times the initial value at room temperature, consistent with findings in other *ex vivo* animal soft tissues (Kiss *et al* 2009). Below  $55\,^{\circ}$ C, changes were moderated, remaining below 50% increase. A moderate correlation was observed between the animal's age and the SWS value at room temperature (Pearson r = 0.5925), older animals showing higher SWS values (see figure 4(a)). However, this moderate correlation disappeared at ablative temperatures (Pearson r = 0.0251 at  $65\,^{\circ}$ C), suggesting that age was not a relevant factor in this study. These findings should be interpreted with caution due to the limited number of samples in each age group. No statistically significant differences were found between the samples obtained from the 'toro de lidia' group and the rest (t-test, p > 0.05) at each registered temperature.

The mechanisms driving stiffness changes during heating are not fully understood but are hypothesized to involve collagen denaturation (Wall *et al* 1999, Wright and Humphrey 2002, Lepetit 2007). At temperatures exceeding 60 °C, collagen fibres contract, transitioning from their native triple-helical structure to a more disordered state, resulting in irreversible stiffness increases. Irreversible changes were observed in test type 3 even at thermal exposures as low as 20 CEM43 min (the test employed a temperature of 43 °C, see figure 6), and the remaining SWS values stabilised post-cooling.

A consistent observation across all tests was the variability in absolute SWS values among samples, which underscores the importance of analysing relative changes rather than relying on absolute measurements. This variability could be attributed to individual differences in tissue composition and anatomy, factors commonly observed in other glandular tissues (Sapin-de Brosses *et al* 2010). Age and breed were not found related to the observed inter-sample variability at thermal injury temperatures.

**IOP** Publishing

The study also pointed out possible limitations of the CEM43 scale. Using the original CEM43 scale by Sapareto and Dewey (1984) yielded unrealistically high values in the order of  $10^{10}$  CEM43 min for bath temperatures exceeding  $50\,^{\circ}$ C. Adopting R based on equation (2) and using experimental data from Bhowmick *et al* (2004), produced more sensible results with established thresholds for thermal injury (in the order of hundreds of CEM43 min (Geoghegan *et al* 2022)), with the largest SWS increments occurring above 200 CEM43 min, as observed in the first type of test (see figure 4(b)).

Although the samples were relatively thin (thickness between 10 and 15 mm) and the region for SWS analysis was located close to the surface, a temperature gradient occurred between the sample surface and core. Therefore, it must be acknowledged that the true temperature at the region of SWS analysis could not be directly measured, which may have affected the actual CEM43 values obtained. This issue becomes even more critical under rapid heating protocols where heating occurs within seconds. Future work on the characterisation of SWS during rapid ablation should address this challenge, for instance by combining experimental data with thermodynamics simulations.

Results from test type 2 under steady temperature showed no significant correlation between temperature and the rate of change in SWS values (Pearson r = 0.4093) (figure 5(b)). Nonetheless, this observation should be interpreted with caution, as the range of temperatures tested was narrow and the number of samples limited. When the same dataset was plotted as a function of thermal dose using the modified CEM43 scale with the parameters from Bhowmick *et al* (2004), two distinct groups emerged (figure 5(c)), separating exposures below and above 50 °C. CEM43 assumes that 43 °C is a pivotal temperature for thermal cytotoxicity. Therefore, the forking most likely arises from the mathematical definition of CEM43 with respect to temperature (equation (1)). The different behaviour of the data when plotted against temperature versus thermal dose (figures 5(b) and (c)) can be attributed to the distinct mechanisms underlying the two biomarkers. The CEM43 scale is based on thermal cytotoxicity, whereas SWS changes induced by heating are mainly linked to alterations in the structural components of the tissue. Further research should examine the correlation between elastography results and cellular viability to validate SWS as a practical biomarker of thermal damage.

Furthermore, no clear thermal exposure threshold for a sharp stiffness increase was identified in the results from test type 2, unlike the findings for muscular tissue under a similar heating protocol (Sapin-de Brosses *et al* 2011). This discrepancy raises questions, as the time profiles reported by Sapin-de Brosses *et al* (2011) do not appear fully consistent with their corresponding CEM43 plots. Furthermore, no transient softening was observed in our samples, contrasting with studies on *ex vivo* bovine muscular tissue (Benech and Negreira 2010, Sapin-de Brosses *et al* 2010) but aligning with *ex vivo* liver tissue behaviour (Kiss *et al* 2009, Sapin-de Brosses *et al* 2010). These differences may be related to the distinct content and organisation of structural proteins across tissue types. Glandular tissues such as liver and prostate differ notably from musculoskeletal tissues in this regard, which could influence their thermomechanical response. In particular, thermal transitions involving partial denaturation and subsequent reorganisation of protein structures—such as collagen (Wright and Humphrey 2002, Lepetit 2007, Sapin-de Brosses *et al* 2010). Although these mechanisms have been more clearly characterised in muscle, they may help explain the monotonic increase in SWS observed. Further investigation, including histological analysis, would be necessary to clarify the structural basis of these findings.

Despite the valuable insights gained, this study presents several limitations. The inter-sample variability observed suggests histological differences among the samples, which were not investigated. Experimental constraints, like impurities accumulating in the water bath in the long-duration test type 2, reduced SNR and prematurely terminated some tests, potentially affecting measurement consistency. Additionally, the *ex vivo* nature of the study excludes the influence of perfusion, a critical factor in *in vivo* thermal ablation.

Overall, the results evidenced a substantial increase in SWS at higher temperatures, especially above 60 °C. The clear differences observed between initial and final SWS values suggest that elastography could delineate thermal ablation lesions. Specifically, applying a defined threshold value indicative of complete coagulative necrosis might assist in differentiating treated from untreated regions, potentially enhancing the precision of thermal ablation procedures. Future research should investigate *in vivo* perfused conditions, correlating elastography results with cellular viability and biological injury to refine and validate SWS as a practical metric. Furthermore, exploring longer-term biomechanical changes postablation and refining thermal dose metrics could significantly advance the interpretation and utility of elastography data.

# 5. Conclusion

This preliminary study investigated the effects of thermal exposure on the elastic properties of prostatic tissue using *ex vivo* bovine samples. Despite significant variability, consistent trends emerged, with substantial SWS increases observed at higher temperatures, particularly above 60°C, where increments of up to fivefold were recorded. These findings encourage further exploration of SWS measurements for identifying and delineating thermal ablation lesions. The results also indicate potential limitations of the CEM43 scale at elevated temperatures, which should be further examined under conditions where core temperature can be more accurately assessed-an aspect that becomes especially critical for rapid thermal ablation protocols. Future research should additionally assess the impact of perfusion on heat deposition and examine the biomechanical response of prostatic tissue under rapid heating protocols that better mimic real thermal ablation conditions.

# Data availability statement

All data that support the findings of this study are included within the article (and any supplementary information files).

# Acknowledgments

A Gomez was supported by the European Commission (Fellowship number HORIZON-MSCA-2021-PF-01-101062897). Further funding was also provided by the University of Granada (Grant Number PPJIA2022-22) and the Spanish Ministry of Science (Grant Number PDC2021-120945-I00). The authors thank the local abattoirs 'El Durqueño' (Santa Fe, Granada, Spain), 'Antonio Luis SL' (Baza, Granada, Spain) and 'Cárnicas Moreno Jiménez' (Alcalá la Real, Jaén, Spain) for providing the animal samples.

#### **ORCID** iDs

Leon Zurfluh © 0009-0001-0067-0691 Antonio Callejas © 0000-0002-8506-5166 Antonio Gomez © 0000-0002-2981-0539

# References

Amador C, Kinnick R R, Urban M W, Fatemi M and Greenleaf J F 2015 Viscoelastic tissue mimicking phantom validation study with shear wave elasticity imaging and viscoelastic spectroscopy 2015 IEEE Int. Ultrason. Symp. IUS 2015 pp 1–4

Arcot R and Polascik T J 2022 Evolution of focal therapy in prostate cancer: past, present and future *Urol. Clin. North Am.* 49 129–52 Arnal B, Pernot M and Tanter M 2011 Monitoring of thermal therapy based on shear modulus changes: I. Shear wave thermometry *IEEE Trans. Ultrason. Ferroelectr. Freq. Control* 58 369–78

Arnal B, Pernot M and Tanter M 2011 Monitoring of thermal therapy based on shear modulus changes: II. Shear wave imaging of thermal lesions *IEEE Trans. Ultrason. Ferroelectr. Freq. Control* 58 1603–11

Assi H T I, Arsenault M G, Whelan W M and Kumaradas J C 2022 A new thermal dose model based on vogel-tammann-fulcher behaviour in thermal damage processes *Int. J. Hyperth.* **39** 697–705

Bamber J et al 2013 EFSUMB guidelines and recommendations on the clinical use of ultrasound elastography. Part 1: basic principles and technology Ultraschall Med. 34 238–53

Basseri S, Perlis N and Ghai S 2024 Focal therapy for prostate cancer Abdominal Radiol. 50 757-69

Benech N and Negreira C A 2010 Monitoring heat-induced changes in soft tissues with 1D transient elastography *Phys. Med. Biol.* 55 1753

Bercoff J, Pernot M, Tanter M and Fink M 2004 Monitoring thermally-induced lesions with supersonic shear imaging *Ultrason. Imaging* 

Bhowmick P, Coad J E, Bhowmick S, Pryor J L, Larson T, Rosette J D L and Bischof J C 2004 *In vitro* assessment of the efficacy of thermal therapy in human benign prostatic hyperplasia *Int. J. Hyperth.* 20 421–39

Curiel L, Souchon R, Rouvière O, Gelet A and Chapelon J Y 2005 Elastography for the follow-up of high-intensity focused ultrasound prostate cancer treatment: initial comparison with MRI *Ultrasound Med. Biol.* 31 1461–8

Dewhirst M W, Viglianti B L, Lora-Michiels M, Hanson M and Hoopes P J 2003 Basic principles of thermal dosimetry and thermal thresholds for tissue damage from hyperthermia *Int. J. Hyperth.* 19 267–94

Geoghegan R, ter Haar G, Nightingale K, Marks L and Natarajan S 2022 Methods of monitoring thermal ablation of soft tissue tumors—a comprehensive review *Med. Phys.* 49 769–91

Gomez A, Rus G and Saffari N 2023 Reverse time migration and genetic algorithms combined for reconstruction in transluminal shear wave elastography: an *in silico* case study *Ultrasonics* 138 107206

Henriques F C and Moritz A R 1947 Studies of thermal injury: I. The conduction of heat to and through skin and the temperatures attained therein. A theoretical and an experimental investigation *Am. J. Pathol.* **23** 530–49

James N D et al 2024 The Lancet commission on prostate cancer: planning for the surge in cases Lancet 403 1683–722

Kiss M Z, Daniels M J and Varghese T 2009 Investigation of temperature-dependent viscoelastic properties of thermal lesions in ex vivo animal liver tissue I. Biomech. 42 959–66

- Lepetit J 2007 A theoretical approach of the relationships between collagen content, collagen cross-links and meat tenderness *Meat Sci.* **76** 147–59
- LeRoy B E and Northrup N 2009 Prostate cancer in dogs: comparative and clinical aspects Veterinary J. 180 149-62
- Li G-Y, Zheng Y, Jiang Y-X, Zhang Z and Cao Y 2019 Guided wave elastography of layered soft tissues Acta Biomater. 84 293-304
- Loupas T, Powers J and Gill R W 1995 An axial velocity estimator for ultrasound blood flow imaging, based on a full evaluation of the doppler equation by means of a two-dimensional autocorrelation approach IEEE Trans. Ultrason. Ferroelectr. Freq. Control 42 672–88
- Mariani A, Kwiecinski W, Pernot M, Balvay D, Tanter M, Clement O, Cuenod C a and Zinzindohoue F 2014 Real time shear waves elastography monitoring of thermal ablation: in vivo evaluation in pig livers J. Surg. Res. 188 37–43
- Mitri F G, Urban M W, Fatemi M, Member S, Greenleaf J F and Fellow L 2011 Shear wave dispersion ultrasonic vibrometry for measuring prostate shear stiffness and viscosity: an *in vitro* pilot study *IEEE Trans. Biomed. Eng.* 58 235–42
- Nightingale K, McAleavey S and Trahey G 2003 Shear-wave generation using acoustic radiation force: *in vivo* and *ex vivo* results *Ultrasound Med. Biol.* **29** 1715–23
- Payen T, Crouzet S, Guillen N, Chen Y, Chapelon J-Y, Lafon C and Catheline S 2024 Passive elastography for clinical HIFU lesion detection *IEEE Trans. Med. Imaging* 43 1594–604
- Sapareto S A and Dewey W C 1984 Thermal dose determination in cancer therapy *Int. J. Radiat. Oncol. Biol. Phys.* 10 787–800 Sapin-de Brosses E, Gennisson J L, Pernot M, Fink M and Tanter M 2010 Temperature dependence of the shear modulus of soft tissues assessed by ultrasound *Phys. Med. Biol.* 55 1701–18
- Sapin-de Brosses E, Pernot M and Tanter M 2011 The link between tissue elasticity and thermal dose *in vivo Phys. Med. Biol.* 56 7755–65
- Scholte J G 1947 The range of existence of rayleigh and stoneley waves *Geophys. Suppl. Mon. Not. R. Astron. Soc.* 5 120–6 Shi W *et al* 2015 Monitoring of radiofrequency ablation with shear wave delay mapping 2015 IEEE Int. Ultrason. Symp. IUS 2015 pp 10–13
- Sigrist R M S, Liau J, Kaffas A E, Chammas M C and Willmann J K 2017 Ultrasound elastography: review of techniques and clinical applications *Theranostics* 7 1303–29
- Souchon R, Rouvière O, Gelet A, Detti V, Srinivasan S, Ophir J and Chapelon J Y 2003 Visualisation of HIFU lesions using elastography of the human prostate *in vivo*: preliminary results *Ultrasound Med. Biol.* **29** 1007–15
- University of Wisconsin-Madison, Department of Animal Sciences n.d. Lecture 3: additional diagrams not found in the text the bull reproductive tract (available at: www.ansci.wisc.edu/jjp1/ansci\_repro/lec/lec3\_male\_anat/lec3diag.html/) (Accessed 24 June 2024)
- van der Poel H G *et al* 2018 Focal therapy in primary localised prostate cancer: the european association of urology position in 2018 *Eur. Urol.* **74** 84–91
- van Rhoon G C 2016 Is cem43 still a relevant thermal dose parameter for hyperthermia treatment monitoring? *Int. J. Hyperth.* 32 50–62 Wall M S, Deng X-H, Torzilli P A, Doty S B, O'Brien S J and Warren R F 1999 Thermal modification of collagen *J. Shoulder Elb. Surg.* 8 339–44
- Wright N T and Humphrey J D 2002 Denaturation of Collagen via Heating: an Irreversible Rate Process Annu. Rev. Biomed. Eng. 4 109–28